The effect of substrate orientation on the kinetics and thermodynamics of initial oxide-film growth on metals

Von der Fakultät Chemie der Universität Stuttgart
zur Erlangung der Würde eines Doktors der Naturwissenschaften (Dr. rer. nat.)
genehmigte Abhandlung

vorgelegt von

Friederike Reichel

aus Aachen

Hauptberichter:	Prof. Dr. Ir. E. J. Mittemeijer
Mitberichter:	Prof. Dr. Dr. h. c. M. Rühle
Prüfer:	Prof. Dr. F. Aldinger
Prüfungsvorsitzender:	Prof. Dr. H. Bertagnolli

Tag der Einreichung:	28.09.2007
Tag der mündlichen Prüfung:	19.11.2007

MAX-PLANCK-INSTITUT FÜR METALLFORSCHUNG STUTTGART
INSTITUT FÜR METALLKUNDE DER UNIVERSITÄT STUTTGART

Stuttgart 2007

Contents

Chapter 7

Summary

This thesis addresses the effect of the parent metal-substrate orientation on the thermodynamics and kinetics of ultra-thin (< 5 nm) oxide-film growth on bare metals upon their exposure to oxygen gas at low temperatures (up to 650 K). As demonstrated, for such thin oxide overgrowths on their metals, the resulting oxide-film microstructures often differ from those predicted by *bulk* thermodynamics, because of the relatively large contributions of interface and surface energies to the total energetics of the various metal-substrate/oxide-film systems (Chapters 2, 3 and 4). Further, surface and interface thermodynamics can stabilize crystallographic orientation relationships (COR) with unexpected high lattice mismatches between the crystalline oxide overgrowth and the metal substrate (Chapter 4). An amorphous state for ultra-thin oxide films grown on e.g. Al, Ta or Si can be thermodynamically, instead of kinetically, preferred up to a certain critical oxide-film thickness, because of the lower sum of surface and interface energies as compared to the corresponding crystalline modification (Chapter 3). Beyond this critical oxide-film thickness, bulk thermodynamics will strive to stabilize the competing crystalline oxide phase, but the corresponding amorphous-to-crystalline transition can then be kinetically hindered by a relatively large energy barrier for nucleation of crystallization (Chapter 5). An amorphous-to-crystalline transition of the developing oxide film will affect the activation-energy barriers for ion and electron transport in the oxide, and thereby govern the oxide-film growth kinetics as function of the oxidation conditions, e.g. oxidation temperature, partial oxygen pressure and parent metal-substrate orientation (Chapter 6).

Apart from the scientific interest to investigate the, up to date largely unaddressed, effect of the parent metal-substrate orientation on the oxidation process, the achieved fundamental knowledge on the oxide-film growth kinetics and microstructure as function of the growth conditions is, at the same time, of great technological importance. For example, the specific properties of thin oxide films (e.g. electric conductivity, wear and corrosion resistance as well as thermal and mechanic stability), as used in numerous technological application areas such as microelectronics, catalysis and surface coatings, will be determined by their microstructure. In particular, the growth of either an amorphous or a coherent, single-

crystalline oxide film is desired, because of the absence of grain boundaries in both these types of oxide films. Grain boundaries in the grown oxide films may act as paths for fast atom or electron transport, thereby deteriorating material properties such as the electrical resistivity, corrosion resistance or catalytic activity. Thus, to further optimize the chemical and physical properties of the applied oxide films, a fundamental and comprehensive knowledge on the thermodynamics and kinetics of the oxide growth process is required.

To this end, a **model description** has been developed to predict the thermodynamically stable microstructure of a thin oxide film grown on its bare metal substrate as function of the oxidation conditions and the substrate orientation (Chapter 2). In the model calculations, the total energetics (i.e. surface, interface and bulk) of two competing oxide microstructures on identical metal substrates are compared, while accounting for the relaxation of elastic growth strain (due to the initial lattice mismatch between the crystalline oxide overgrowth and its metal substrate) by the introduction of misfit dislocations at the metal/oxide interface. The thermodynamic model can be applied to oxide-overgrowth/metal-substrate systems with low and high initial lattice mismatches and for oxide-film thicknesses from the (sub-) monolayer up to the micrometre range.

The model has been applied to predict whether a thin amorphous oxide film (instead of the competing crystalline modification) can be thermodynamically preferred up to a certain critical thickness for various metal/oxide systems (i.e. of Al, Cu, Ni, Cr, Fe, Mg, Zr, Ti and Si; Chapter 3). It follows that the critical oxide-film thickness, $h^{\text{critical}}_{\{M_x\text{O}_y\}}$, up to which an amorphous oxide overgrowth on its metal substrate is thermodynamically preferred, is governed by: (*i*) the difference in bulk Gibbs energies between the amorphous and competing crystalline oxide phase, (*ii*) the difference in surface energies between the amorphous and competing crystalline oxide overgrowth (as determined by the COR between the crystalline oxide overgrowth and its metal), (*iii*) the strength of the metal-oxygen bond for the metal/oxide system under investigation and (*iv*) the difference in the density of metal-oxygen bonds across the metal/oxide interface between the amorphous and competing crystalline oxide overgrowth (as also determined by the COR between the crystalline oxide overgrowth and its metal). Beyond this critical oxide-film thickness, the competing crystalline oxide overgrowth will be thermodynamically preferred, because the positive bulk Gibbs energy difference between the amorphous and the crystalline oxide overgrowth is no longer overcompensated by the more negative sum of the surface and interfacial energy differences. It follows that amorphous oxide overgrowths on Si are stable up to a thickness in the range of

40 – 80 nm (as dependent on the growth temperature and the substrate orientation). The corresponding critical oxide-film thicknesses are in the range of only several oxide monolayers (ML) on the various low-index crystallographic faces of Al, Ti and Zr, as well as on the less densely packed surfaces of Fe and Cr. For Mg and Ni, the critical oxide-film thickness is less than 1 oxide ML and therefore the initial development of an amorphous oxide phase on these metal substrates is unlikely. Finally, for Cu and densely packed Cr and Fe metal surfaces, oxide overgrowth is predicted to proceed by the direct formation and growth of a crystalline oxide phase (corresponding to a negative critical thickness value; see Fig. 7.1). These results are in qualitative agreement with the scarce number of experimental observations of the initial oxide-film microstructure on metals reported in the literature. Unfortunately, for most metal/oxide-film systems, detailed knowledge on the development of the microstructure of the initial oxide overgrowth on its bare metal (as obtained by e.g. high-resolution electron microscopy) lacks.

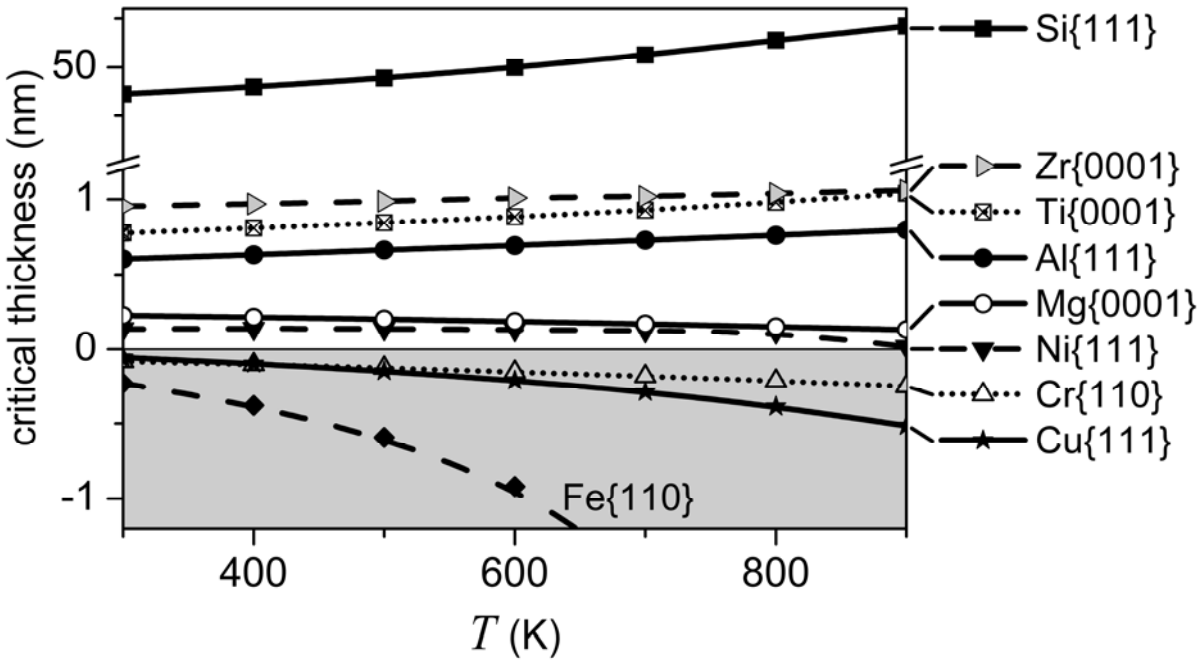

Figure 7.1. Critical thickness up to which an amorphous oxide overgrowth (instead of the corresponding crystalline oxide overgrowth) is thermodynamically preferred on the most densely packed face of a bare metal substrate as function of the growth temperature (*T*) for various metal/oxide systems.

In Chapter 4, the striking **experimental** observation and thermodynamic explanation of a COR of exceptionally high lattice mismatch between a Al{100} metal substrate metal and its crystalline Al_2O_3 overgrowth is reported, which is in contrast with the general assumption that a COR corresponding with low lattice mismatch is always preferred. To this

end, polished Al single-crystals with {111}, {100} and {110} surface orientations were introduced in an ultra-high vacuum (UHV) system for specimen processing and analysis, which consists of three coupled UHV chambers: (*i*) a UHV chamber for analysis by angle-resolved X-ray photoelectron spectroscopy (XPS), (*ii*) a UHV chamber for specimen processing (e.g. surface cleaning, annealing and oxidation) and analysis by the low energy electron diffraction (LEED) and real-time in-situ spectroscopic ellipsometry (RISE) and (*iii*) a UHV chamber for thin film deposition by molecular beam epitaxy (MBE). The introduced Al single-crystals were first cleaned and outgassed by a treatment of sputter cleaning using 1 keV Ar^+ ions and simultaneous annealing at temperatures up to 450°C, while employing sample rotation to avoid sputter-induced roughening of the sample surface. After a final step of in-situ UHV annealing for 15 min at 450°C (without sputter cleaning), the obtained *bare* Al substrates are clean at their surfaces (as verified by AR-XPS) and the crystal order at their surfaces is also fully restored (as verified by LEED). Next, the bare Al substrates have been oxidized by exposure to pure oxygen gas for t = 6000 s in the temperature regime of T = 350 – 650 K at partial pressure of oxygen of p_{O_2} = 1×10^{-4} Pa. During the oxidation, the oxide-film growth kinetics has been established by RISE. After the oxidation, the oxide-film microstructure (e.g. thickness, composition, phase constitution, crystallinity, morphology and local chemical state of the ions) were investigated by AR-XPS and LEED. Finally, high-resolution transmission electron microscopic (HR-TEM) analysis was applied to study the microstructure and morphology of the grown oxide films on an atomic scale, as well as to establish the CORs between the crystalline oxides overgrowths and the parent metal substrates. To this end, some of the grown oxide films were sealed prior to their removal from the UHV system (i.e. prior to their exposure to atmospheric conditions) by deposition of an Al capping layer by MBE, after which a cross-sectional TEM lamella was cut from the specimens by a focussed ion beam (FIB).

Pronounced dependencies of the microstructural evolution and the growth kinetics of the oxide films on the parent metal-substrate orientation are established (see what follows). **The oxide films grown on Al{111}** for t = 6000 s and $T \leq 600$ K are overall stoichiometric (i.e. Al_2O_3) and have uniform thicknesses in the range of L = 0.6 – 0.9 nm (as determined by AR-XPS, RISE and/or HR-TEM). Furthermore, the corresponding metal/oxide interfaces are atomically flat (as evidenced from the cross-sectional HR-TEM analysis). The oxide films grown on Al{111} are amorphous up to T = 450 K, whereas at higher temperatures ($T \geq 475$ K) epitaxial crystalline oxide films with a coherent metal/oxide interface develop (as

evidenced by LEED and HR-TEM; see Fig. 7.2 and Chapter 4). The amorphous oxide films on Al{111} are stable upon subsequent in-situ UHV annealing at 700 K. The thicknesses of these thermally stable, low-T amorphous Al_2O_3 films on Al{111} are in good agreement with the corresponding calculated critical thickness of $h^{\text{critical}}_{\{Al_2O_3\}}$ = 0.7 ± 0.1 nm up to which an amorphous Al_2O_3 film is thermodynamically preferred on the Al{111} substrate. The transformation of the low-T amorphous oxide films into a crystalline Al_2O_3 phase beyond the critical thickness is possibly kinetically hindered by a relatively large energy barrier for nucleation of crystallization.

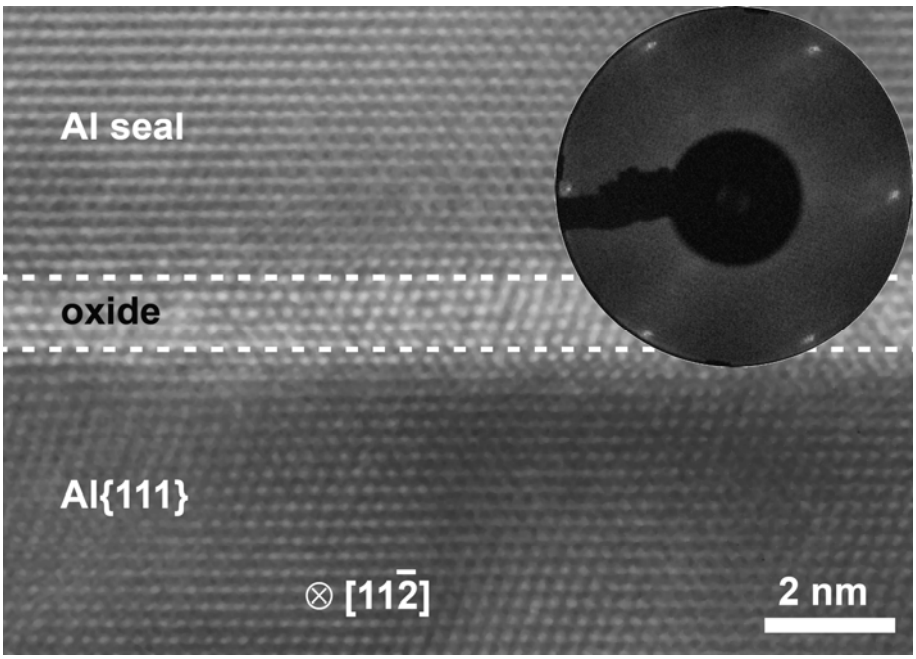

Figure 7.2. High-resolution transmission electron micrograph of the crystalline Al_2O_3 overgrowth on Al{111} after oxidation at T = 550 K and p_{O_2} = 1×10^{-4} Pa for t = 6000 s. The direction of the primary electron beam was along the zone axis [11$\bar{2}$] of the Al{111} substrate, the oxide film and the Al seal. The dashed lines roughly indicate the boundaries between the oxide and the Al{111} substrate and the oxide and the Al seal, respectively. The inlet shows the corresponding LEED pattern (as recorded with a primary electron energy of 53 eV) with a six-fold symmetry due to the epitaxial overgrowth of γ"-Al_2O_3 on Al{111}.

At more elevated temperatures $T \geq 475$ K, an epitaxial crystalline Al_2O_3 film develops on Al{111} instead, because (*i*) the critical oxide-film thickness for the amorphous-to-crystalline transition has decreased as a result of a change in oxide growth mode (from layer-by-layer to island-by-layer growth) and/or (*ii*) oxygen incorporation predominates over on-top oxygen chemisorption for $T \geq 475$ K, thereby reducing the activation-energy barrier for nucleation of crystallization (Chapter 5). The resulting crystalline oxide, designated as γ"-

Al_2O_3 in this thesis, possesses an fcc oxygen sublattice structure with a lattice parameter similar to that of γ-Al_2O_3, but with a random distribution of cations in the interstices of the oxygen sublattice. For the crystalline γ"-Al_2O_3 overgrowth on Al{111}, the expected COR of lowest possible mismatch (~ 2 – 3%) between the Al{111} substrate and the γ"-Al_2O_3 overgrowth is found: Al(111)[$1\bar{1}0$]||γ"-Al_2O_3(111)[$1\bar{1}0$], with a coherent metal/oxide interface (Chapter 4).

The oxide films grown on Al{100} for t = 6000 s and $T \leq 600$ K are also overall stoichiometric (i.e. Al_2O_3) have uniform thicknesses in the range of L = 0.5 – 0.8 nm and atomically flat metal/oxide interfaces. The oxide films grown on Al{100} are amorphous up to T = 400 K, but are transformed into γ"-Al_2O_3 upon subsequent in-situ UHV annealing beyond an experimentally determined critical thickness of 0.45 ± 0.15 nm, which is somewhat lower than the corresponding calculated critical thickness of $h^{\text{critical}}_{\{Al_2O_3\}}$ = 0.8 ± 0.1 nm. At more elevated temperatures T > 400 K, a crystalline γ"-Al_2O_3 film with a semi-coherent metal/oxide interface develops beyond a critical thickness of about 0.2 ± 0.1 nm (as determined experimentally at T = 550 K). The relatively lower value of the critical oxide-film thickness on Al{100} for T > 400 K (as compared to the corresponding critical thickness value for $T \leq$ 400 K) is attributed to a change in oxide growth mode from layer-by-layer to island-by-layer growth (Chapter 5). For the crystalline γ"-Al_2O_3 overgrowth on Al{100}, an unexpected COR of high lattice mismatch (> 15%) between the Al{100} substrate and the γ"-Al_2O_3 overgrowth is found: Al(100)[011]||γ''-Al_2O_3(111)[$01\bar{1}$], with a semi-coherent metal/oxide interface (see Fig. 7.3 and Chapter 4). The crystalline oxide overgrowth structure consists of two types of γ"-Al_2O_3 domains with their {111} plane parallel to the surface, but rotated with respect to each other by 90° around the surface normal. As evidenced by the smearing out in rings of the LEED spots originating from the γ"-Al_2O_3 domains, relaxation of the anisotropic, tensile, elastic growth strain in the oxide overgrowth does not only occur by the formation of defects at the metal/oxide interface (presumably misfit dislocations), but also by slight, in-plane rotations of the γ"-Al_2O_3 domains (of about ± 4º) with respect to the aforementioned high-mismatch COR.

This striking observation of a COR of exceptionally high lattice mismatch between a metal substrate and its oxide overgrowth is in contrast with the general assumption that a COR corresponding with low lattice mismatch is preferred. However, as demonstrated here by thermodynamic model calculations (Chapter 4), the relatively large energy contributions due to residual growth strain and misfit dislocations in such thin overgrowths can be

overcompensated by the relatively low sum of the surface and interface energies. Neglecting the role of the surface energy and/or the interface energy contributions, can therefore lead to wrong theoretical predictions of CORs for ultra-thin overgrowths (Chapter 4).

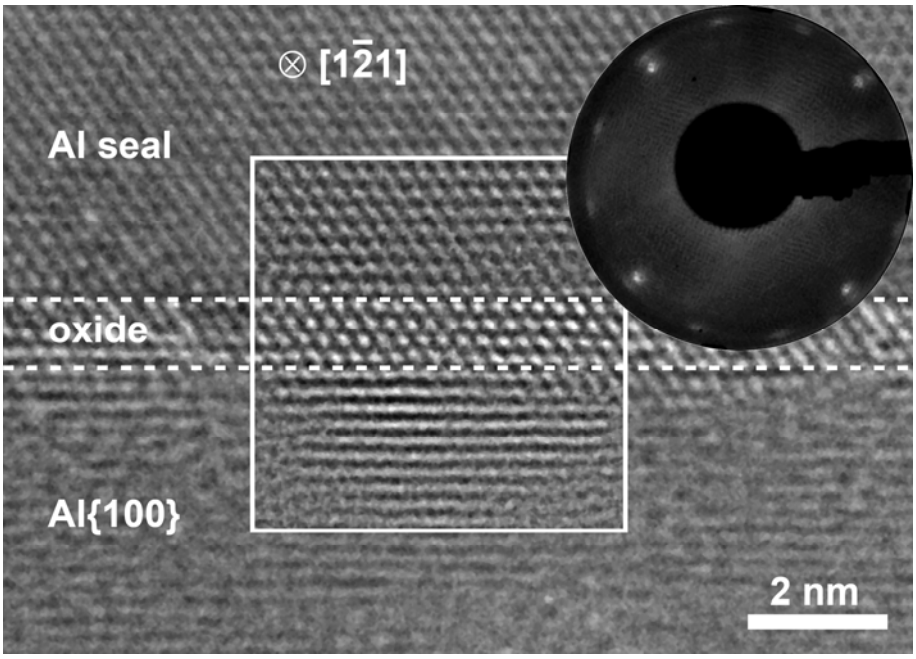

Figure 7.3. High-resolution transmission electron micrograph of the Al_2O_3 overgrowth on Al{100} after oxidation at T = 550 K and p_{O_2} = 1×10^{-4} Pa for t = 6000 s. The direction of the primary electron beam was along the zone axis $[1\bar{2}1]$ of the Al capping layer and the oxide film. The area in the square represents a Fourier-filtered region of the original micrograph. The corresponding LEED pattern for t = 120 s (as recorded with a primary electron of energy 54 eV) shows the separate diffraction spots originating from the Al{100} substrate (exhibiting a four-fold symmetry) and due to the two-domain structure of the γ''-Al_2O_3 oxide overgrowth (exhibiting a twelve-fold symmetry with spots located in rings).

The oxide films grown on Al{110} for t = 6000 s and $T \leq$ 550 K are also overall stoichiometric with uniform average thicknesses in the range of L = 0.6 – 1.2 nm. The oxide films are amorphous and stable upon subsequent in-situ UHV annealing at 700 K, in accordance with the relatively high value of the calculated critical oxide-film thickness on Al{110} of $h^{\text{critical}}_{\{Al_2O_3\}}$ = 4.0 ± 0.5 nm. At more elevated temperatures T > 550 K, the oxide-film thickness after t = 6000 s increases significantly up to L = 2.75 ± 0.3 nm at T = 640 K and then distinct LEED spots appear at the onset of oxidation, which become weaker with increasing oxidation time. As evidenced by the HR-TEM and LEED analysis, the original bare Al{110} surface becomes reconstructed at the onset of oxidation. As demonstrated by thermodynamic model calculations (Chapter 5), the resulting {111}- faceted oxidized metal

surface is thermodynamically preferred due to the relatively lower energy of the Al{111}/*am*-Al_2O_3 interface (as compared to the Al{110}/*am*-Al_2O_3 interfacial energy). The oxide film grown on Al{110} after prolonged oxidation at 640 K still appears predominantly amorphous in the HR-TEM analysis, which indicates that the amorphous-to-crystalline transition beyond the critical oxide-film thickness is kinetically hindered (Chapter 5).

The **kinetics of the oxide-film growth** on the bare Al{100} and Al{110} substrates in the temperature range of 350 – 600 K at p_{O_2} = 1×10^{-4} Pa, as experimentally established by RISE, can be subdivided into a initial, very fast and a subsequent, very slow oxidation stage, which is characterized by the occurrence of a near-limiting thickness that increases with increasing temperature (see Fig. 7.4). For the oxidation of the bare Al{111} substrate up to T = 450 K, a distinction between an initial, very fast and a subsequent, very slow oxidation stage cannot be made (see Fig. 7.4a). Instead, the initial oxide-film growth rate on Al{111} decreases only gradually with increasing oxidation time without the attainment of a near-limiting oxide-film thickness and an unexpected decrease of the oxide-film thickness with increasing T after t = 6000 s of oxidation is observed for $T \leq 450$ K (i.e. within the amorphous temperature regime). At higher temperatures $T > 450$ K (i.e. within the crystalline temperature regime), the growth kinetics on Al{111} can also (as for Al{100} and Al{110}, see Fig. 7.4 b) be subdivided into an initial, very fast and a subsequent, very slow oxidation stage with a near-limiting thickness that increases with increasing temperature (Chapter 6).

The experimental growth curves for the thermal oxidation of Al single-crystals in the temperature regime of 350 – 600 K can be accurately described by considering the coupled currents of Al^{3+} cations and electrons (by both thermionic emission and quantum mechanical tunnelling) in an uniform surface-charge field and taking the rate-limiting activation energy for cation transport, W, and the work-function difference, $\Delta\chi$, (i.e. the difference between the work-functions at the oxide/oxygen and oxide/metal interface) as fit parameters (see Fig. 7.4). It follows that the oxide-film growth rate is always limited by the diffusion of cations through the developing oxide film under influence of the surface charge field setup by chemisorbed oxygen species at the growing oxide-film surface. Electron transport is co-determining the oxide growth rate only at the onset of oxidation. The kinetic potential due to the surface-charge field is maintained during continued oxide-film growth by the (near-) balance between a very large, forward electron flux by tunnelling and a slightly smaller, reverse electron flux by thermionic emission.

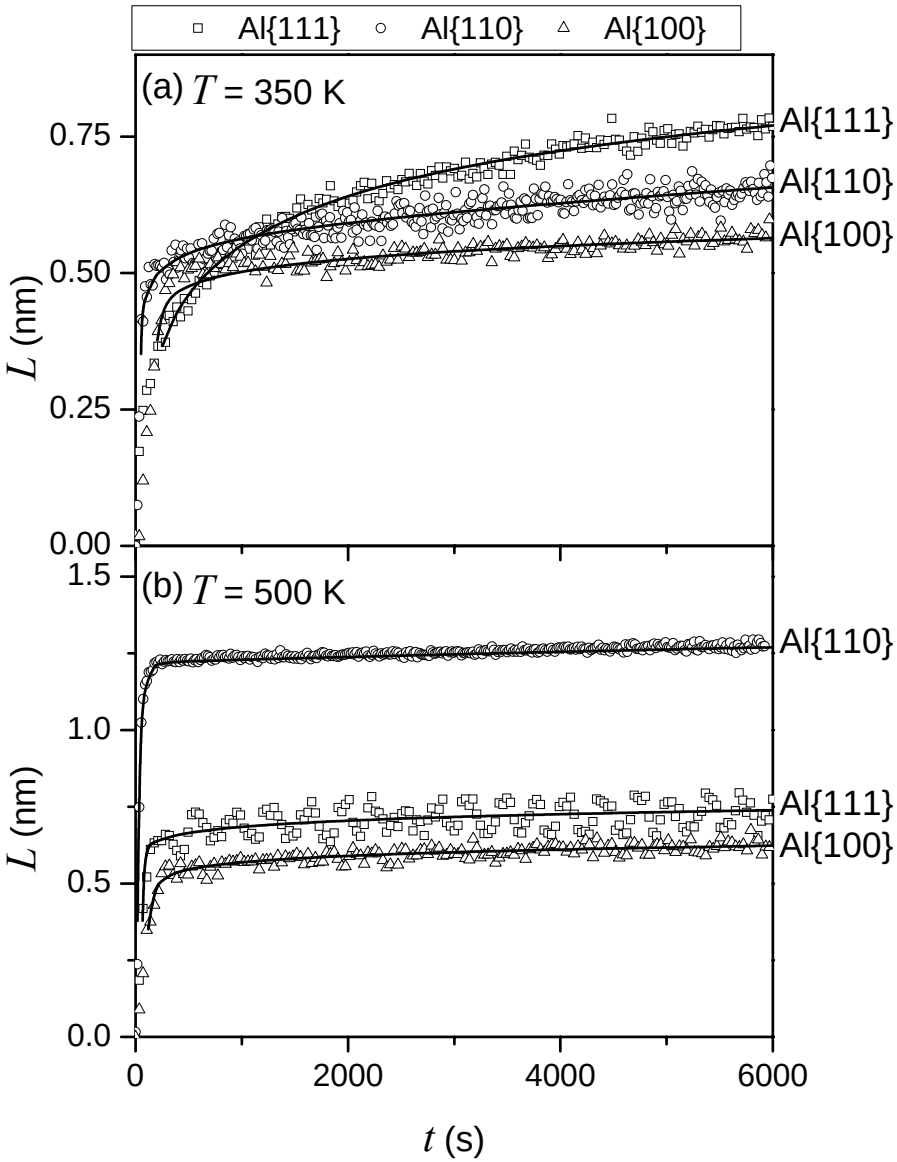

Figure 7.4. Experimental (*open markers*) and model fitted (*lines*) oxide-film growth curves for the oxidation of bare Al{111} (*squares*), Al{100} (*circles*) and Al{110} (*triangles*) substrates at (**a**) $T = 350$ K and (**b**) $T = 500$ K (all at $p_{O_2} = 1\times10^{-4}$ Pa). The experimental data has been obtained by RISE. The theoretical growth curves have been calculated on the basis of the coupled currents of cations and electrons (by both tunnelling and thermionic emission) under a surface-charge field.

Due to the gradual transformation of the initial amorphous oxide film on Al{100} into γ"-Al_2O_3, the energy barrier for cation transport and the absolute value of the kinetic potential both increase gradually with increasing oxidation temperature in the range of 350 – 600 K for Al{100}, as well as up to 450 K for Al{110}. The relatively large energy barrier for cation transport together with the decrease of the surface-charge field strength with increasing oxide-film thickness leads to the observed initial, very fast and subsequent, very slow oxidation stage and the occurrence of a near-limiting oxide-film thickness that increases with increasing

temperature. On Al{111}, the corresponding amorphous-to-crystalline transition occurs toward higher temperatures $T > 450$ K and is more abrupt (than for Al{100} and Al{110}). Consequently, the value of the energy barrier for cation transport is relatively low within the amorphous temperature regime up to $T = 450$ K, resulting in a more gradual growth mode without the establishment of a near-limiting oxide-film thickness in the amorphous temperature regime (i.e. for $T \leq 450$ K). Around the amorphous-to-crystalline transition temperature for Al{111}, the corresponding values of the energy barrier for cation transport and the kinetic potential abruptly change towards the corresponding values for the crystalline oxide films grown on Al{100} and Al{110} and then the growth behaviour becomes independent of the metal-substrate orientation.

It is concluded that the parent metal-substrate orientation plays a decisive role for the kinetics and thermodynamics of the oxidation process. A comprehensive description of the thermodynamics of ultra-thin oxide overgrowth on bare metal substrates can only be achieved if the role of surface and the interface energy contributions is accounted for. Fundamental understanding of the initial oxide-film growth kinetics on bare metal surfaces, on the other hand, requires detailed knowledge on the microstructural evolution of the developing oxide film as function of the oxidation conditions.